Analysis of the spreading width of the particle-hole giant resonances

G. G. Dussel*
Departamento de Física, FCEyN, Universidad de Buenos Aires, Pabellón 1, Ciudad Universitaria, 1428 Buenos Aires, Argentina

E. C. Seva and H. M. Sofia
Departamento de Física, Comisión Nacional de Energía Atómica, Avenida del Libertador 8250, 1429 Buenos Aires, Argentina
(Received 16 March 1993)

We evaluate the spreading width of the giant resonances using the discontinuity in the second derivative of the propagator of the vibrational phonon. This allows us to isolate the processes that contribute to the spreading width in terms of the Feynman diagrammatic expansion of the full boson propagator. Utilizing for classification purposes the nuclear field theory perturbative treatment of the one-phonon state, we obtain a very simple expression for the spreading width in the lowest (nonvanishing) order of perturbation theory.

PACS number(s): 21.60.Jz, 21.10.Re

I. INTRODUCTION

The giant multipole resonances can be thought of macroscopically as vibrations of the nuclear surface and are strongly populated in experiments involving photoabsorption or inelastic scattering of alphas, ^{3}He, and protons. They are produced by the promotion of nucleons across the Fermi surface to unoccupied major valence shells and can be described microscopically as coherent particle-hole excitations that exhaust a large portion of the sum rule for multipole electric or magnetic operators. The contribution of processes that are partially in the continuum has attracted interest due to possibilities of measuring and calculating partial widths [1–7].

The centroid of the distributions of multipole strength can be taken into account through a random phase approximation (RPA) calculation, which provides a representation of the excitation energy of the corresponding collective state. These calculations successfully reproduce the experimental data, linking each giant mode to the corresponding term of the nucleon-nucleon interaction.

The mixture of the collective state with more complicated nuclear configurations appearing at similar energies is beyond the framework of the RPA calculations because it involves states with two-particle–two-hole (2p-2h), (3p-3h), etc.

The damping of the giant resonance collective motion is due mainly to three processes, for which considerable effort has been devoted: (a) The Landau damping in the finite nucleus or the fragmentation of the resonance over the RPA configurations. (b) The escape width related to direct particle emission [1–4] is frequently associated with the portion of the giant resonance (GR) having the particle (of the particle-hole pair) in the continuum [8–12]. (c) The spreading width, related to the second moment $\mu^{(2)}$ of the strength distribution, provides instead a direct measure of the leading-order admixture of the collective mode with neighboring more complicated configurations, mainly 2-particle–2-hole states. Considerable work has been done on this subject using pure 2p-2h configurations [13–19] or approaching the 1p-1h collective state with one- and two-phonon configurations [20–25]. These ideas have been used within the consistent Green's function method [26] and in a simple model using nuclear field theory (NFT) [22,27]. This model [22,27] underestimates the spreading width by a factor of 2 as is indicated in Ref. [25].

In this paper, we develop a method to calculate the spreading width based on the time evolution [28] of the collective degrees of freedom, which leads to a particularly simple diagrammatic expansion for the second moment of the strength distribution. In our method we worked on the one- and two-phonon configurations. In nuclear field theory (NFT) [29] a simple two-level model (the Lipkin model) is used for classification purposes. In this model there are two levels of degeneracy 2Ω with an energy separation ϵ, and the particles interact via a particle-hole monopole interaction that scatters particles from the lower level to the higher one and vice versa.

NFT gives a good prescription for treating collective states as bosonic degrees of freedom, even if they have been built from fermionic degrees of freedom through a RPA or Tamm-Dancoff approximation (TDA) treatment. In this framework, the bosons and the fermions are treated on an equal footing and any physical observable can be calculated using a perturbative diagrammatic expansion and a set of well prescribed rules. In this way, any physical calculation can be done perturbatively up to the desired order in Ω. The price that has to be paid in order to use this method is to work on an overcomplete

*On leave of absence from the Comisión Nacional de Energía Atómica.

basis and to define a NFT Hamiltonian in which one adds to the original one a collective single-boson Hamiltonian and a particle-boson interaction (Fig. 1).

One of the rules of the NFT allows only one fermionic line in the initial or final states, avoiding in this way overcompleteness of the basis. However, this rule is not fulfilled by the intermediate states which are defined in an overcomplete space of fermions and bosons. This leads to two kinds of problems: (a) The mixture of the collective state with states of more than one coherent fermionic pair is not clear because of the overcompleteness of the intermediate basis. (b) The minimum number of vertices that contribute to the perturbative expansion is three, because two of them are needed in going from the bosonic state to the fermionic pair. As the number of time ordering diagrams is equal to $n!$, where n the number of vertices, this implies that the number of diagrams to be calculated increases rapidly. That is even worse due to the two types of vertices (fermionic and particle-boson) that are included in the NFT Hamiltonian.

It must be noted, nevertheless, that the vertices of Fig. 1(a) must not be considered as interactions, but only as amplitudes of the fermionic pair in the collective state.

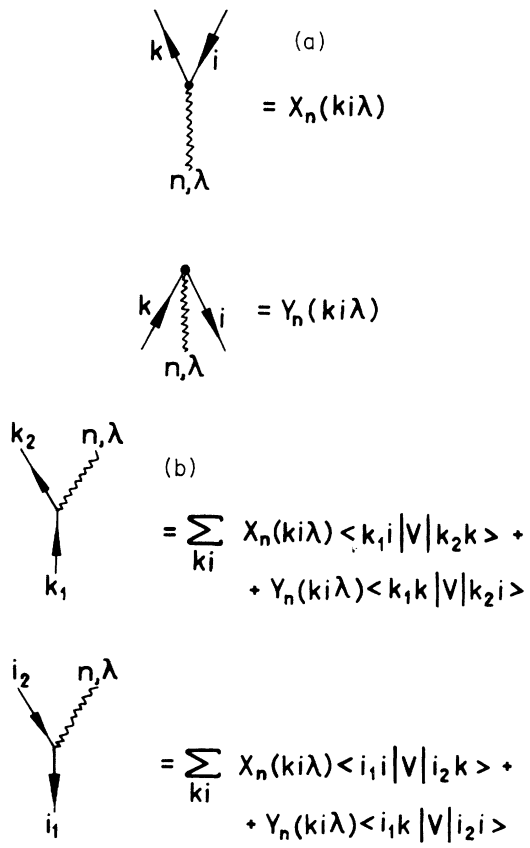

FIG. 1. List of the particle-boson vertices. In our model, the NFT vertices shown in (a) are not considered interactions but rather the forward and backward amplitudes of the boson and are represented by heavy dots. Instead, the scattering vertices of (b) are real interactions that change the number of bosons by ± 1.

For example, consider a particle-hole RPA creation operator

$$\Gamma_n^\dagger = \sum_{k,i} X_n(k,i) a_k^\dagger a_i - Y_n(k,i) a_i^\dagger a_k \ , \tag{1.1}$$

where k denotes states above the Fermi surface, i states below the Fermi surface, and $a^\dagger$ the operator that creates a particle in a given state. The NFT interactive vertices of Fig. 1(a) are replaced by

$$\begin{aligned} \langle \Gamma_n | a_k^\dagger a_i \rangle &= X_n(k,i) \ , \\ \langle \Gamma_n | a_i^\dagger a_k \rangle &= Y_n(k,i) \ . \end{aligned} \tag{1.2}$$

These are not interaction vertices of the Hamiltonian and consequently do not have an intermediate time in a Feynman diagrammatic expansion. In this way, the diagrams needed to calculate the admixture of two-boson states in a one-boson state are reduced drastically, and they are the only ones that contribute to the spreading width of the collective state in leading order.

For a weak interaction (where the strength parameter is smaller than the critical one), NFT demonstrates that for a system formed by 2Ω particles (i.e., the lower level filled), the energy of the ground state has a Hartree contribution proportional to Ω, the Fock terms give a contribution of order 1, and the RPA (without exchange) is also of order 1, while the exchange terms of the RPA yield contributions of order $1/\Omega$ and higher in this parameter. All the other contributions can be classified in terms of different powers of $1/\Omega$, if the collective excitation is described by a nonexchange RPA.

It has been found in real calculations that a classification in terms of different powers of $1/\Omega$ is meaningful. For example, in the calculation of the energy associated with the two-pair addition (^{212}Pb) and two-pair removal (^{204}Pb) [30], the $1/\Omega$ contributions were smaller than 10% of the terms of order 1, and the $(1/\Omega)^2$ terms yielded contributions less than 10% of those of order $1/\Omega$. It is necessary to be rather careful in summing up all the diagrams of a given order, because there could be very large cancellations. It has been found to be a better approximation not to consider at all some diagrams of an order of perturbation theory rather than to include only some of the contributing diagrams.

In this spirit, we will study which are the processes that contribute in the lowest nonvanishing order (which turns out to be order $1/\Omega$) to the spreading width. We will see, moreover, that these contributions can be summed up to a very simple expression and that will be the main result of the present paper. It is worthwhile to remark that NFT will be used to isolate the diagrams that contribute to the first order in $\frac{1}{\Omega}$, and also to evaluate them.

In Sec. II, we will review the relevant points related to the width of the collective excitations and to their calculation in the TDA. In Sec. III, we discuss some physical properties that can be extracted from the short-time behavior of the collective-state Green's function and its derivatives, with special emphasis on the results relevant to the RPA. We will also calculate the first-order contribution (in terms of $\frac{1}{\Omega}$) to the spreading width of a collective state.

In the Appendix, we described a calculation in a two-level model that shows which are the processes (or diagrams), in the leading order of the NFT framework, that are taken into account by our calculation of the spreading width of the one-phonon state.

II. STATEMENT OF THE PROBLEM AND THE SPREADING WIDTH OF PARTICLE-HOLE TDA COLLECTIVE STATES

Let H be a Hamiltonian matrix with elements h_{ij} and U the unitary matrix that brings H to its diagonal form with eigenvalues E_i. The matrix U is built from the eigenvectors of H. Then the following equations hold:

$$HU = UE, \qquad U^\dagger U = 1 ,$$
$$\sum_j h_{ij}u_{jk} = u_{ik}E_k , \tag{2.1}$$

and thus

$$H = UEU^\dagger = M(E) ,$$
$$h_{ij} = \sum_k (u_{ik})^2 E_k = \sum_k u_{ik}E_k u^*_{ki} . \tag{2.2}$$

Equation (2.2) is just an energy-weighted sum rule for the eigenvector components u_{ik}, relating the unperturbed energies contained in h_{ii} to the final eigenvalues E_k. We see that the weighted average of the final eigenvalues is given by the diagonal matrix element h_{ii} that is composed only by the bare single-boson energy ω_i. Introducting the 2p-2h states changes the next moment of the strength distribution through the off-diagonal terms of the Hamiltonian matrix. To see this, we note that

$$(H)^2 = (UEU^\dagger UEU^\dagger) = (UE^2U^\dagger) = M(E^2) . \tag{2.3}$$

Thus the second moment associated with the ith unperturbed state is

$$\mu_i^{(2)} = (UE^2U^\dagger)_{ii} - (UEU^\dagger)^2_{ii} = \sum_{k\neq i} h^2_{ki} . \tag{2.4}$$

It is conceptually helpful to develop a perturbative interpretation of $\mu_i^{(2)}$ [31]. For this purpose, we analyze the Brillouin-Wigner (BW) perturbative expansion of the state $|i\rangle$ with energy ω_i. This amounts to solving the equation

$$E = f_i(E) , \tag{2.5}$$

with

$$f_i(E) = \omega_i + \langle i|V\frac{1}{E-H_0}(1-|i\rangle\langle i|)V|i\rangle + \langle i|V\frac{1}{E-H_0}(1-|i\rangle\langle i|)V\frac{1}{E-H_0}(1-|i\rangle\langle i|)V|i\rangle + \cdots$$
$$= \omega_i + \sum_{k\neq i}\frac{V^2_{ik}}{E-\omega_k} + \sum_{kr\neq i}\frac{V_{ik}V_{kr}V_{ri}}{(E-\omega_k)(E-\omega_r)} + \cdots . \tag{2.6}$$

In (2.6) we have assumed that the Hamiltonian splits into an unperturbed (diagonal) H_0 and a perturbation V that couples the state $|i\rangle$ to more complicated configurations $k, r, \ldots$ We further assumed that any diagonal contribution V_{ii} has been already absorbed into ω_i.

It can clearly be seen, by straightforward application of the Cauchy theorem, that

$$\mu_i^{(2)} = \frac{1}{2i\pi}\int_c f_i(z)dz = \sum_{k\neq i} V^2_{ik} , \tag{2.7}$$

where c is a closed contour in the complex energy plane that encircles all eigenvalues of H_0. We thus conclude that $\mu_i^{(2)}$ is uniquely determined by the second (in power of V) order in the BW perturbative expansion.

More complicated configurations, entering in higher orders of the BW expansion, only change higher-order moments. This amounts to stating that the details of the strength distribution will change upon the inclusion of such terms, but in such a way that the average Gaussian envelope remains the same. This is schematically displayed in Fig. 2.

The arguments that we have presented can be applied to the evaluation of the spreading width of a collective particle-hole excitation assuming that the boson basis is not overcomplete. That is the case of the TDA bosons, at least in a first-order approximation. The RPA bosons, on the other hand, form an overcomplete basis due to ground-state correlations and will be treated in the next section.

The TDA boson is defined by

$$|\lambda, n\rangle = \sum_{ki} X_{\lambda,n}(ki)[c^\dagger_k c_i]_\lambda . \tag{2.8}$$

As we have already seen, the only contributions to $\mu^{(2)}$ are from the matrix elements involving the first power of the two-body interaction and having the giant resonance $|\lambda, n\rangle$ as initial state. Since these can only connect $|\lambda, n\rangle$ with states of two-particle–two-hole structure, the only matrix element that survives is

$$\langle \lambda_1 n_1, \lambda_2 n_2|H|\lambda n\rangle = \sum_{k's,i's} X_{\lambda_1,n_1}(k_1i_1)X_{\lambda_2,n_2}(k_2i_2)X_{\lambda,n}(ki)\langle k_1i_1, k_2i_2|H|ki\rangle \tag{2.9}$$

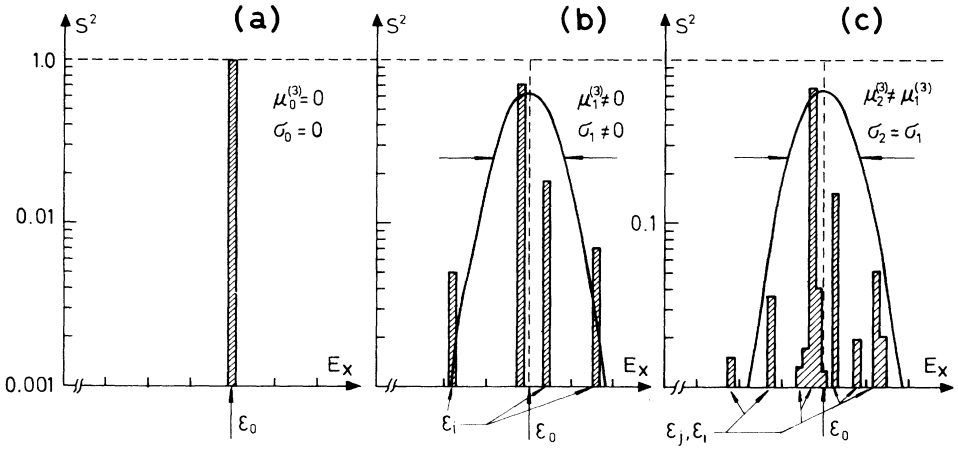

FIG. 2. Schematic illustration of the successive corrections to the one-boson propagator and the corresponding fragmentation of the strength function. (a) The zeroth order in the BW expansion corresponds to the bare energy of the boson without any fragmentation. (b) In the next order, some strength is transferred to the intermediate configuration with energy E_k. These are enveloped by a Gaussian with a width given by $\sigma_1 \neq 0$. (c) The higher-order corrections change the details of the strength distribution, and the width σ remains unchanged, but $\mu^{(3)}$, the third moment of the strength distribution, changes.

and the spreading width is

$$\sigma^2 = \mu^{(2)} = \sum_{\lambda_1 n_1, \lambda_2 n_2} (\langle \lambda_1 n_1, \lambda_2 n_2 | H | \lambda n \rangle)^2 \ . \quad (2.10)$$

In Eq. (2.9) we define an energy-independent vertex between one- and two-boson states. This is diagrammatically represented in Fig. 3.

III. SPREADING WIDTH OF A PARTICLE-HOLE RPA COLLECTIVE STATE AND THE SHORT-TIME BEHAVIOR OF THE GREEN'S FUNCTION

The arguments of the previous section have to be used cautiously when trying to evaluate the spreading width in the RPA. In this case, the basis is overcomplete because the RPA ground state has an undefined number of bosons and is due to the simultaneous consideration of fermion and boson excitations. We therefore prefer to work directly with the Feynman- Goldstone diagrams, through a perturbative expansion of the one-boson Green's function. In Ref. [28], it was shown that there exists a direct relation between the matrix elements of different powers of the Hamiltonian and the short-time behavior of the derivatives of the Green's function. We start by defining a Hamiltonian of the system that can be split into a one-boson Hamiltonian H_0 and a perturbation H_1,

$$H_0 = H_{\mathrm{RPA}} + h \ ,$$
$$H_1 = V - h \ , \quad (3.1)$$

where H_{RPA} is the one-RPA-boson Hamiltonian while h is an arbitrary one-boson potential that contains all the residual interactions or Pauli corrections that can mix the different roots of the RPA. V is the rest of the interaction of a general two-body force. We will start from the boson representation $|n\rangle$ that diagonalizes H_0.

The one-phonon Green's function, corresponding to the total Hamiltonian [Eq. (3.1)] in the Lehmann representation, is given by the following equation:

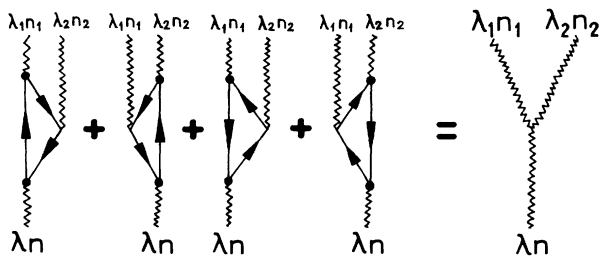

FIG. 3. Two-body matrix elements (including direct and exchange parts) that are relevant to the admixture of one and two TDA bosons. Diagrammatic representation of Eq. (2.9) in the text. Heavy dots represent the amplitudes X.

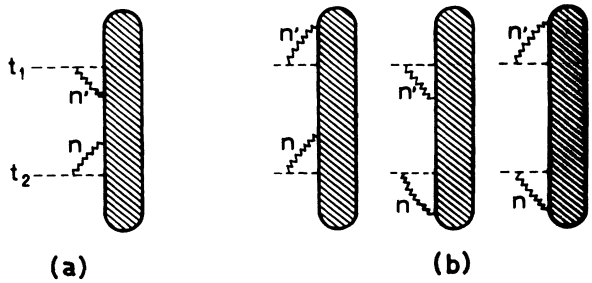

FIG. 4. General form of Feynman-Goldstone diagrams contributing to the one-boson Green's function. (a) Schematic representation of restricted diagrams. (b) The same for unrestricted diagrams.

$$G(n,n';t_2-t_1) = \langle\Psi_0|T[\Gamma_{n'}(t_2)\Gamma_n^\dagger(t_1)]|\Psi_0\rangle$$
$$= \sum_m \langle\Psi_0|\Gamma_n|\psi_m\rangle\langle\psi_m|\Gamma_{n'}^\dagger|\Psi_0\rangle e^{-iW_m(t_2-t_1)}\theta(t_2-t_1)$$
$$+ \sum_{\bar{m}} \langle\Psi_0|\Gamma_{n'}^\dagger|\psi_{\bar{m}}\rangle\langle\psi_{\bar{m}}|\Gamma_n|\Psi_0\rangle e^{-iW_m(t_1-t_2)}\theta(t_1-t_2), \quad (3.2)$$

where $\Gamma_n^\dagger$ creates a RPA boson with quantum numbers $\{n\}$ and RPA energies ω_n, while W_m are the excitations energies for the eigenstates ψ_m of the total Hamiltonian.

As we are interested in a diagrammatic expression for $\mu^{(2)}$ we can utilize the expansion in Feynman diagrams of the Green's function (see Fig. 4),

$$G(n,n';t_2-t_1) = G_0(n;t_2-t_1)\delta_{n,n'} + \int d\tau d\tau' \sum_m G_0(n;\tau-t_1)F(n,m;\tau'-\tau)G(m,n';t_2-\tau') \ , \quad (3.3)$$

where $F(n,m;\tau'-\tau)$ is the self-energy of the problem and is represented by the same diagrams of Fig. 4 without the external lines. $G_0(n;t_2-t_1) = e^{-i\omega_n(t_2-t_1)}\theta(t_2-t_1)$ is the bare RPA-boson Green's function for positive energies.

The diagrams that are relevant here are time diagrams rather than energy diagrams (time running upwards), where in the blobs could be anything including the vertices of the Hamiltonian that introduce the ground-state fluctuations.

Looking at the definition of the second moment of the strength function [Eq. (2.4)], we see that the second derivative minus the square of the first derivative is the only contribution to the spreading width.

In Ref. [28], it is shown that a lot of relevant information can be obtained by looking at the short-time behavior of the Green's function and its derivatives near $t_2 - t_1 = 0$,

$$\frac{\partial^n}{\partial t^n}G(n,n';t)\Big|_{t\to 0^+} - \frac{\partial^n}{\partial t^n}G(n,n';t)\Big|_{t\to 0^-} \ . \quad (3.4)$$

Following Ref. [28] we classify the Feynman-Goldstone diagrams as two types: (a) Restricted diagrams [Fig. 4(a)]. These are the diagrams that have a continuous chain of boson and fermion lines, where the intermediate times are always between t_1 and t_2, i.e.,

$$t_1 < \tau < \tau' < \cdots < t_2$$

or

$$t_1 > \tau > \tau' > \cdots > t_2 \ .$$

(b) Unrestricted diagrams [Fig. 4(b)]. In these diagrams, the intermediate times do not follow the above rules. Therefore, all such diagrams are continuous as $t_1 \to t_2$, and do not contribute to the discontinuity at $t_2 = t_1$.

The restricted diagrams, instead, exist only for $t_2 > t_1$ or $t_1 > t_2$. If the chain contains more than one link, each integration produces a factor $t_2 - t_1$ when $t_2 \to t_1$. Therefore, it can be easily seen that the contribution to the nth derivative is given only by the restricted diagrams that have a maximum of n intermediate times (or vertices). For example, the contribution to the discontinuity of the Green's function comes only from the discontinuity of the bare Green's function [see Eq. (3.3)] because none of the diagrams of the Feynman expansion gives any contribution, i.e.,

$$G(n,n';t_2-t_1)|_{t_2-t_1\to 0^+} - G(n,n';t_2-t_1)|_{t_2-t_1\to 0^-}$$
$$= [G_0(n,;t_2-t_1)|_{t_2-t_1\to 0^+} - G_0(n;t_2-t_1)|_{t_2-t_1\to 0^-}]\delta_{n,n'} = \delta_{n,n'} \ , \quad (3.5)$$

given a normalization condition for the "strength distribution" of the bare boson state in the eigenstates of the total Hamiltonian.

In the same way we treated the Green's function, we can study the discontinuity of its first time derivative. To obtain the Feynman expansion of $G'(n,n',t)$, we have to calculate $G(n,n';t+dt) - G(n,n',t)$ and divide the result by dt. This leads to the result

$$i\frac{\partial}{\partial t_2}G(n,n';t_2-t_1) = \omega_{n'}G(n,n';t_2-t_1) + B(n,n';t_2-t_1) \ , \quad (3.6)$$

where $B(n,n';t_2-t_1)$ involves the same diagrams as in Fig. 4, except that they terminate at the time t_2 with a vertex. In a complete basis, this vertex cannot be any of the interactions that have already been taken into account in the RPA formalism.

The discontinuity of the first derivative can be calculated as the difference between $G'(n,n';t_2-t_1)$ for $t_2-t_1 \to 0^+$ and $G'(n,n';t_2-t_1)$ for $t_2-t_1 \to 0^-$:

$$
\begin{aligned}
&i\frac{\partial}{\partial t_2}G(n,n';t_2-t_1)\Big|_{t_2-t_1\to 0^+} - i\frac{\partial}{\partial t_2}G(n,n';t_2-t_1)\Big|_{t_2-t_1\to 0^-} \\
&\quad = \sum_m W_m\left[\langle\Psi_0|\Gamma_n|\psi_m\rangle\langle\psi_m|\Gamma^+_{n'}|\Psi_0\rangle - \sum_{\bar{m}}\langle\Psi_0|\Gamma^+_{n'}|\psi_{\bar{m}}\rangle\langle\psi_{\bar{m}}|\Gamma_n|\Psi_0\rangle\right] \\
&\quad = \omega_n\delta_{n,n'} + B(n,n';t_2-t_1=0)\ ,
\end{aligned}
\tag{3.7}
$$

where some of the diagrams that contribute to $B(n,n',t_2-t_1=0)$ are shown in Fig. 5.

It can be seen that this discontinuity takes into account the fact that the energy centroid of the dressed bosons is equal to the bare energy of the boson plus contributions coming either from the residual interaction between the particle and the hole of the boson (not taken into account by the RPA) or from the one-vertex interaction between the boson and the correlated ground state.

Furthermore, the right-hand side of Eq. (3.7) is the matrix element of the total Hamiltonian between two different roots of the RPA equation. This means that the diagrams of Fig. 5 do not mix the one-boson state with states of more than one boson, since states that appear diagrammatically with more than one particle-hole pair at a given time are produced by the ground-state fluctuations:

$$
\langle n|H|n'\rangle = \omega_n\delta_{n,n'} + B(n,n';t_2-t_1=0)\ . \tag{3.8}
$$

This property has been pointed out in Ref. [31] and has been utilized in Ref. [28] to explain the sum rule of spectroscopic factors for single-fermion energies and in Ref. [32] to obtain the first-order energy-weighted sum rule for bilinear operators.

In the same way, we can examine the discontinuity of the second derivative of the Green's function:

$$
\begin{aligned}
\langle n|H^2|n\rangle &= \Big(\lim_{t_2-t_1\to 0^+} - \lim_{t_2-t_1\to 0^-}\Big)\frac{\partial^2}{\partial t_2\partial t_1}G(n,n;t_2-t_1) \\
&= \sum_m W_m^2\langle\Psi_0|\Gamma_n|\psi_m\rangle\langle\psi_m|\Gamma^+_n|\Psi_0\rangle - \sum_{\bar{m}} W_{\bar{m}}^2\langle\Psi_0|\Gamma^+_n|\psi_{\bar{m}}\rangle\langle\psi_{\bar{m}}|\Gamma_n|\Psi_0\rangle\ .
\end{aligned}
\tag{3.9}
$$

In order to obtain a relation between the above equation and the diagrammatic expansion, we must study the second derivative of the Feynman expansion of the Green's function:

$$
\frac{\partial^2}{\partial t_2\partial t_1}G(n,n;t_2-t_1) = \omega_n^2 G(n,n;t_2-t_1) + \omega_n B(n,n;t_2-t_1) + \omega_n C(n,n;t_2-t_1) + D(n,n;t_2-t_1)\ , \tag{3.10}
$$

where $B(n,n;t_2-t_1)$ involves the diagrams finishing with an interactive vertex at t_2, defined before and shown in Fig. 4; $C(n,n;t_2-t_1)$ is the same but beginning with the vertex at t_1, and $D(n,n;t_2-t_1)$ involves those diagrams with two vertices, one at each time (Fig. 6). The last set of diagrams can be split in two parts, those that pass by an intermediate state equal to the initial one [Fig. 6(a)] and those in which none of the intermediate states are equal to the initial one [Fig. 6(b)].

The discontinuity at $t_2-t_1=0$ of the three first terms of Eq. (3.10) plus the discontinuity of the diagrams of $D(n,n,t_2-t_1)$ that can be divided in two by cutting those intermediate states that are the same as the initial state produce a contribution equal to $\langle n|H|n\rangle^2$.

Finally, the only contribution to the second moment of

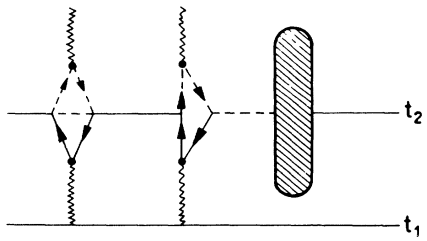

FIG. 5. Schematic representation of the diagrams finishing with a vertex at time t_2, included in $B(n,n';t_2-t_1)$. The representation of fermions by dashed lines implies that their propagator must not be included. They are utilized for labeling the matrix element. The blob can be anything provided it is linked to the initial boson.

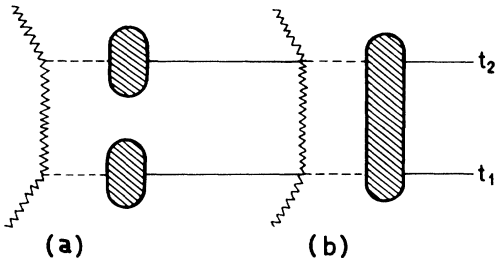

FIG. 6. Schematic representation of the diagrams finishing with two vertices, one at time t_2 and the other at time t_1, included in $D(n,n';t_2-t_1)$. (a) Diagrams that can be divided in two by cutting the intermediate state whenever they are the same as the initial states. (b) Diagrams where this division is not possible.

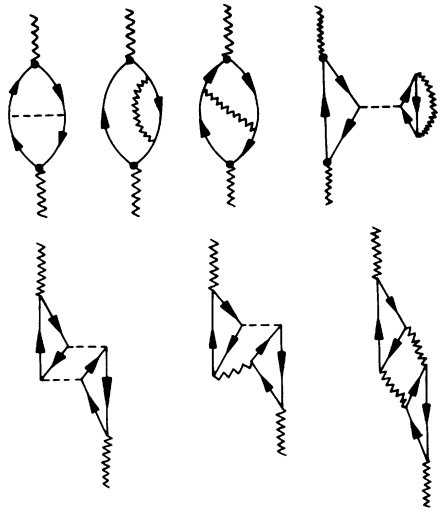

FIG. 7. Diagrams that contribute to the energy of one-boson states in the leading order $(1/\Omega)$. All the time ordering of the vertices must be included in the calculation. In the figure, we have shown only one of the possible time orderings for simplicity.

the strength distribution comes from the discontinuity of those diagrams that begin and end with an interaction and have no intermediate state equal to the initial one, because these contribute to $(\langle n|H|n\rangle)^2$ and are canceled in the subtraction. It is worth noting that in the limit $t_2 - t_1 = 0$, the two vertices occur at the same time and there is no propagator between them, giving a contribution equal to the product of the two matrix elements.

In the NFT framework, the diagrams contributing to the leading-order correction to the energy of the one-boson state are shown in Fig. 7. However, not all of them contribute to the calculation of $\mu^{(2)}$. The diagrams relevant to the calculation of $\mu^{(2)}$ are those that have two interactions changing the number of bosons (or particle-hole pairs) by ± 1 linked to the initial or final boson line.

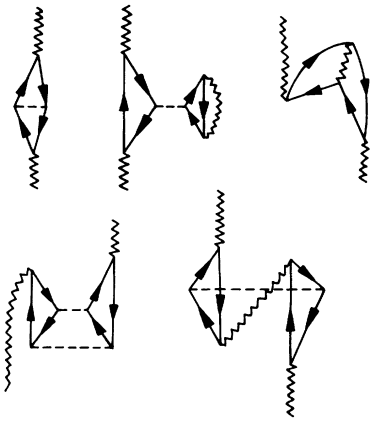

FIG. 8. Some of the diagrams that contribute to the change in the energy of the RPA boson without contributing to its spreading width.

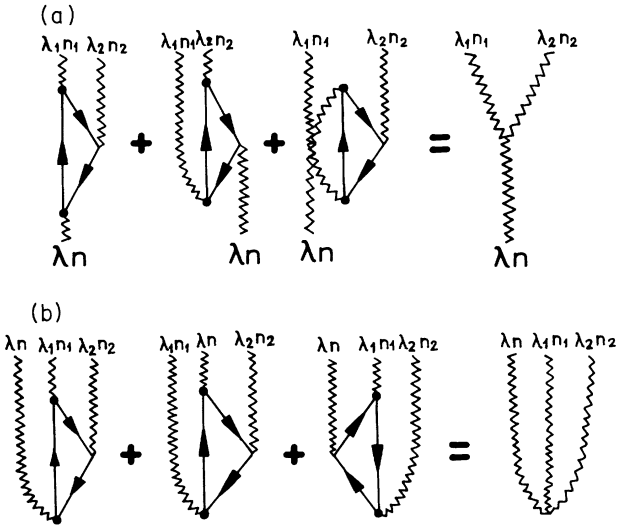

FIG. 9. Two-body matrix elements (including direct and exchange parts) that are relevant to the admixture of one and two RPA bosons. (a) Diagrammatic representation of the forward vertex Eq. (3.11) and (b) of the backward vertex Eq. (3.12). Heavy dots represents the forward (backward) amplitudes X (Y) of the RPA bosons.

These vertices must act at times which are between the annihilation of the initial boson and the creation of the final one. Figure 7 includes these types of diagrams but part of them only moves the energy of the one-boson state without changing its strength distribution. Examples of these diagrams are shown in Fig. 8.

It is not simple to see from these diagrams that the intermediate state is a two-boson state, because of ground-state fluctuations. Otherwise, within our method, the contribution of these diagrams to the discontinuity of the Green's function is reduced to the square of the matrix

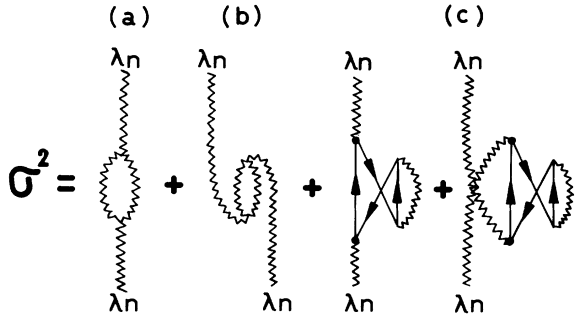

FIG. 10. Schematic representation of the contributions to the square of the spreading width (second moment of the strength function). It must be remembered that the two vertices occur at the same time, which implies that there is no propagator between them. It means that these diagrams have no energy denominators. (a) Contributions from the forward one-boson–two-boson matrix element. (b) Contributions from the backward one-boson–two-boson matrix element. (c) Correction to the spreading width due to the first-order Pauli correction of the RPA one-boson wave function.

element between one-boson and two-boson states.

We can conclude by saying that the only intermediate states that can be reached from the one-boson state through the two-body interaction and contribute to the leading order in perturbation theory are those shown in Fig. 9. Those shown in Fig. 9(b) are related to the backward vertex of the RPA and are not present in the TDA. The corresponding vertices are

$$\langle \lambda_1 n_1, \lambda_2 n_2 | H | \lambda n \rangle = \sum_{j_1 j_2 j_3} \{ [X_n(j_1 j_2 \lambda) X_{n_1}(j_1 j_3 \lambda_1) + Y_n(j_1 j_2 \lambda) Y_{n_1}(j_1 j_3 \lambda_1)] \times \Lambda_{n_2}(j_2, j_3, \lambda_2) + X_{n_2}(j_2 j_3 \lambda_2) Y_{n_1}(j_1 j_3 \lambda_1) \Lambda_n(j_1, j_2, \lambda) \} \times \sqrt{(2\lambda_1+1)(2\lambda_2+1)} (-)^{j_1+j_3+\lambda_2+\lambda} \begin{Bmatrix} \lambda & \lambda_1 & \lambda_2 \\ j_3 & j_2 & j_1 \end{Bmatrix} \sqrt{1+\delta_{n_1 n_2}} , \tag{3.11}$$

$$\langle [\lambda_1 n_1, \lambda_2 n_2]_\lambda \lambda n | H | 0 \rangle = \sum_{j_1 j_2 j_3} \{ [X_n(j_1 j_2 \lambda) Y_{n_1}(j_1 j_3 \lambda_1) + X_{n_1}(j_1 j_2 \lambda) Y_n(j_1 j_3 \lambda_1)] \times \Lambda_{n_2,}(j_2, j_3, \lambda_2) + Y_{n_2}(j_2 j_3 \lambda_2) X_{n_1}(j_1 j_3 \lambda_1) \Lambda_n(j_1, j_2, \lambda) \} \times \sqrt{(2\lambda_1+1)(2\lambda_2+1)} (-)^{j_1+j_3+\lambda_2+\lambda} \begin{Bmatrix} \lambda & \lambda_1 & \lambda_2 \\ j_3 & j_2 & j_1 \end{Bmatrix} \sqrt{1+\delta_{n_1 n_2}} , \tag{3.12}$$

where $X_n(ki\lambda)$ is the RPA forward amplitude and $Y_n(ki\lambda)$ is the RPA backward amplitude, while the scattering matrix element Λ is [29]

$$\Lambda_n(j, j', \lambda) = \sum_{ki} [X_n(ki\lambda) \langle ji | V | j'k \rangle + Y_n(ki\lambda) \langle jk | V | j'i \rangle] . \tag{3.13}$$

The label k denotes states above the Fermi surface and i those below.

It is important to note that the scattering matrix element changes sign depending whether the levels j's correspond to particles or holes.

There still exists an additional contribution to the spreading width due to a Pauli correction between the particle (hole) of the initial boson and the ground state [Fig. 10(c)]. These, in fact, contribute to the width of the single-particle states and, thus, to the width of the RPA collective states. If we take into account all the contributions, the spreading width to first order in $\frac{1}{\Omega}$ is given by

$$\sigma^2 = \mu^{(2)} = \sum_{n_1 n_2 \lambda_1 \lambda_2} [(\langle \lambda_1 n_1, \lambda_2 n_2 | H | \lambda n \rangle)^2 + (\langle [\lambda_1 n_1, \lambda_2 n_2]_\lambda \lambda n | H | 0 \rangle)^2] - \sum_{n_1 \lambda_1} \sum_{j_1 j_2 j_3} \{ [X_n(j_1 j_2 \lambda)]^2 + [Y_n(j_1 j_2 \lambda)]^2 \} \frac{2\lambda_1 + 1}{2j_2 + 1} [\Lambda_{n_1}(j_2 j_3 \lambda_1)]^2 . \tag{3.14}$$

This is our final expression for the spreading width and it is summarized in Fig. 10. It takes into account all the contributions coming from the NFT diagrams up to first order in the parameter $1/\Omega$. It depends only on the two-body interaction and on the collectivity of the two bosons that mix with the giant resonance.

IV. CONCLUSIONS

There are many different approaches to evaluate the spreading width but in almost all of them the physics is very similar: The spreading width is due to the mixture between the coherent one–particle-one-hole state and more complicated structures.

It is well know that if the ground-state correlations are not considered then the spreading width can be obtained exactly in terms of the admixture between the giant resonance and the two-particle–two-hole states (see for instance Ref. [31]).

The problems gets more complicated when there are ground-state correlations. Here the correlations are taken into account by using an effective Hamiltonian that couples the one-boson state to two-boson states and the ground state to the three-boson states. In Ref. [21] this approach has been used to obtain an effective dispersion relation for the collective sates. This way not only is the spreading width obtained but also the Landau damping is included in a very natural way. Another possibility is to consider "dressed" one-particle–one-hole states that include a configuration more complicated than the usual RPA (see, for example, the treatments developed in Refs. [24] and [12]).

In this paper we have proposed a simple version of the spreading width for the giant resonance that corresponds to the leading order (in terms of $\frac{1}{\Omega}$) obtained when the spreading width is evaluated in the framework of NFT. Our result must be compared with similar results obtained using the same framework [22,27]. In their approach, which uses a mixture basis of collective RPA bosons and particle-hole states, at least some diagrams that take into account ground-state correlations are ne-

glected [for example, the last term of Eq. (3.14) is absent]. We worked in a complete basis of only RPA bosons and show explicitly that all the contributions of this order in NFT have been included. It is also possible to extend our method to finite temperature in a similar way to what has been done, for example, in Ref. [33]. It is important to remark that to consider only the $\frac{1}{\Omega}$ terms is a reasonable approximation since usually it is enough to get an estimate of the order of magnitude when evaluating the spreading width.

This work was supported by the Consejo Nacional de Investigaciones Científicas y Técnicas.

APPENDIX

In this appendix we show that the diagrams relevant to the calculation of the spreading width can be interpreted as the square of the matrix element of one-boson and two-boson states.

The model considered in Ref. [29] consisted of two single-particle levels, each with degeneracy 2Ω and a monopole particle-hole interaction that couples the particles in the two levels. A closed-shell nucleus is simulated by considering a system of 2Ω particles in the lower level and the upper one empty:

$$H = H_{\rm SP} - \frac{V}{2}Q^2 \ . \tag{A1}$$

Because of the presence of scattering terms in the monopole interaction, the initial Hamiltonian does not satisfy the Hartree-Fock minimization condition. Consequently, a Hartree-Fock transformation between single-particle states was carried out, in yielding a new Hamiltonian, that can be treated with a diagrammatic expansion:

$$\begin{aligned} H &= H_{\rm SP} + H_q + U \ , \\ H_{\rm SP} &= \epsilon_1 N_1 - \epsilon_{\bar 1} N_{\bar 1} \ , \\ H_q &= -\frac{V}{2}(A^{\dagger 2} + 2A^\dagger A + A^2) - V[A^\dagger(q_1 N_1 - q_{\bar 1} N_{\bar 1}) + (q_1 N_1 - q_{\bar 1} N_{\bar 1})A] - \frac{V}{2}[(q_1 N_1 - q_{\bar 1} N_{\bar 1})^2 - (q_1^2 N_1 - q_{\bar 1}^2 N_{\bar 1})] \ , \end{aligned} \tag{A2}$$

where U is the Hartree-Fock contribution to the ground-state energy and is not important in the calculation of the excited RPA energies, q_1 ($q_{\bar 1}$) are the single-particle (single-hole) monopole moments, and $A^\dagger$, N_1, and $N_{\bar 1}$ are defined by

$$A^\dagger = \sum_m c^\dagger_{m1} c_{m\bar 1}, \qquad N_1 = \sum_m c^\dagger_{m1} c_{m1}, \qquad N_{\bar 1} = \sum_m c^\dagger_{m\bar 1} c_{m\bar 1} \ . \tag{A3}$$

Following closely the NFT calculation [29], we define an adimensional parameter

$$x = \frac{4V\Omega}{\epsilon}, \qquad \epsilon = \epsilon_1 - \epsilon_{\bar 1} \ . \tag{A4}$$

In this way all the physical observables can be written as a polynomial in x.

The construction of the phonon is done through a RPA formalism. In this case, only one collective state is obtained with energy and forward and backward amplitudes given by

$$\begin{aligned} \omega &= \epsilon\sqrt{(1-x)} \ , \\ X &= \langle 1|c^\dagger_{m1} c_{m'\bar 1}|0\rangle = \frac{(\epsilon+\omega)}{2\sqrt{2\epsilon\omega\Omega}}\delta_{m,m'} \ , \\ Y &= \langle 1|c^\dagger_{m'\bar 1} c_{m1}|0\rangle = \frac{(\epsilon-\omega)}{2\sqrt{2\epsilon\omega\Omega}}\delta_{m,m'} \ . \end{aligned} \tag{A5}$$

NFT introduces collective and particle-vibration Hamiltonians that produce new vertices and allow a diagrammatic perturbative treatment of the problem:

$$\begin{aligned} H_{\rm NFT} &= H_{\rm SP} + H_q + \omega\Gamma^\dagger\Gamma + H_{\rm PV} + U \ , \\ H_{\rm PV} &= -\Lambda(\Gamma^\dagger + \Gamma)(A^\dagger + A + q_1 N_1 + q_{\bar 1} N_{\bar 1}) \ , \end{aligned} \tag{A6}$$

where Λ is obtained from the normalization condition of the phonon,

$$\Lambda = V2\Omega(X+Y) \ . \tag{A7}$$

All the vertices of the NFT interaction are defined by the Hamiltonian of Eq. (A6). The calculation of the diagrams is now straightforward following the rules of NFT. In Ref. [29], the leading-order ($\frac{1}{\Omega}$) contribution to the energy of the one-boson state, including all terms up to x^3, was calculated. We have extended the calculation up to the next order (x^4) in order to take into account the leading-order contributions of all the $\frac{1}{\Omega}$ diagrams which are relevant for the calculation of $\mu^{(2)}$, shown in Fig. 6, and which is given by

$$\Delta E = \frac{\epsilon x^2}{16\Omega}\left(1 + x + \frac{9}{8}x^2\right) - \frac{\epsilon x^2}{4\Omega}(q_1 - q_{\bar 1})^2\left(1 + \frac{3}{2}x + \frac{9}{4}x^2\right) + \cdots \ . \tag{A8}$$

We can recalculate this up to the same order in perturbation theory, utilizing the matrix elements between one-phonon and two-phonon states [Eqs. (3.11), (3.12)] and the diagrams of Fig. 10(c) [third term in Eq. (3.14)]. In the two-level model, the matrix elements of Eq. (3.11) and Eq. (3.12) are

$$\langle 1|H|2\rangle = (X^2 + Y^2 + XY)\Lambda 2\Omega\sqrt{2}(q_1 - q_{\bar{1}}) ,$$
$$\langle 0|H|3\rangle = -3XY\Lambda 2\Omega\sqrt{2}(q_1 - q_{\bar{1}}) , \tag{A9}$$

where the $\sqrt{2}$ comes from the normalization of the two-boson state. Using these given matrix elements, we calculate the contribution to the energy of the one-boson state, up to the same order in $1/\Omega$ and x, and obtain

$$E_1 = \frac{|\langle 1|H|2\rangle|^2}{(\omega - 2\omega)} = -\frac{|\langle 1|H|2\rangle|^2}{\omega} = -\frac{\epsilon x^2}{4\Omega}(q_1 - q_{\bar{1}})^2\left(1 + \frac{3}{2}x + \frac{33}{16}x^2\right) ,$$
$$E_2 = -\frac{|\langle 0|H|3\rangle|^2}{(3\omega)} = -\frac{3\epsilon x^4}{64\Omega}(q_1 - q_{\bar{1}})^2 . \tag{A10}$$

In addition, the diagrams of Fig. 10 contribute an amount

$$E_3 = -\frac{(X^2 + Y^2)\Lambda^2 2\Omega}{(\omega - 3\omega)} = \frac{\epsilon x^2}{16\Omega}\left(1 + x + \frac{9}{8}x^2\right) . \tag{A11}$$

The sum of the three contributions is

$$\Delta E = E_1 + E_2 + E_3 = \frac{\epsilon x^2}{16\Omega}\left(1 + x + \frac{9}{8}x^2\right) - \frac{\epsilon x^2}{4\Omega}(q_1 - q_{\bar{1}})^2\left(1 + \frac{3}{2}x + \frac{9}{4}x^2\right), \tag{A12}$$

which is the same result as was obtained within the NFT formalism [Eq. (A8)]. This demonstrates that our method of constructing the matrix elements between one and two RPA bosons is correct and that mixing one-boson states with more complicated configurations produces the spreading width. The additional contributions coming from the diagrams of Fig. 10 are due to the width of the single-particle (-hole) states from which the boson has been built. They incorporate the Pauli corrections between these fermionic states and those coming from the ground-state correlations.

[1] A. van der Woude, Prog. Part. Nucl. Phys. **18**, 17 (1987).
[2] S. Brandenburg, W. Borghols, A. Drentje, A. van der Woude, M. Harakeh, L. Ekström, A. Hakanson, L. Nilsson, N. Olsson, and R. De Leo, Phys. Rev. C **39**, 2448 (1989).
[3] S. Brandenburg, W. Borghols, A. Drentje, L. Ekström, M. Harakeh, A. van der Woude, A. Hakanson, L. Nilsson, N. Olsson, M. Pignanelli, and R. De Leo, Nucl. Phys. **A466**, 29 (1987).
[4] A. Bracco, J. Beene, N. Van Giai, P.F. Bortignon, F. Zardi, and R. Broglia, Phys. Rev. Lett. **60**, 2603 (1988).
[5] N. Van Giai and Ch. Stoyanov, Phys. Lett. B **252**, 9 (1990).
[6] F. Zardi and P. Bortignon Europhys. Lett. **1**, 281 (1986).
[7] T. Vertse, P. Curutchet, R. Liotta, J. Bang, and N. Van Giai, Phys. Lett. B **264**, 1 (1991).
[8] R. De Haro, S. Krewald, and J. Speth, Nucl. Phys. **A388**, 265 (1982).
[9] P. Curutchet, T. Vertse, and R. Liotta, Phys. Rev. C **39**, 1020 (1989).
[10] T. Vertse, P. Curutchet, and R.J. Liotta, Phys. Rev. C **42**, 2605 (1990).
[11] E. Maglione, R.J. Liotta, and T. Vertse, Phys. Lett. B **298**, 1 (1993).
[12] S. Kammerdzhiev, J. Speth, G. Tertychny, and T. Tselyaev, Nucl. Phys. **A555**, 90 (1993).
[13] A. Adachi and Nguyen Van Giai, Phys. Lett. B **149**, 447 (1984).
[14] J. Sawicki, Nucl. Phys. **23**, 285 (1961).
[15] W. Knüpfer, R. Frey, A. Friebel, W. Mettner, D. Meuer, A. Richter, E. Spamer, and O. Titze, Phys. Lett. **77B**, 367 (1978).
[16] B. Schweisiger and J. Wambach, Nucl. Phys. **A426**, 253 (1984).
[17] S. Drozdz, S. Nishizaki, J. Speth, and J. Wambach, Phys. Rep. **197**, 1 (1990).
[18] K. Takayanagi, K. Shimizu, and A. Arima, Nucl. Phys. **A477**, 205 (1988).
[19] B.A. Rumyantsev and S.A. Kheifets, Yad. Fiz. **21**, 510 (1975) [Sov. J. Nucl. Phys. **21**, 267 (1975)].
[20] F.A. Zivopistsev, N. El Nagar, K.V. Shitikova, N.P. Yudin, and M.Y. Akbary, Phys. Lett. **31B**, 347 (1970).
[21] V.G. Soloviev, Ch. Stoyanov, and A.I. Vdovin, Nucl. Phys. **A288**, 376 (1977).
[22] G.F. Bertsch, P.F. Bortignon, R.A. Broglia, and C.H. Dasso, Phys. Lett. **80B**, 161 (1979).
[23] J.S. Dehesa, J. Speth, and A. Faessler, Phys. Rev. Lett. **38**, 208 (1977).
[24] J. Wambach, V.K. Mishra, and Chu-Hsia Li, Nucl. Phys. **A380**, 285 (1982).
[25] G.F. Bertsch, P.F. Bortignon, and R.A. Broglia, Rev. Mod. Phys. **55**, 287 (1983).
[26] S.P. Kamerdzhiev, Yad. Fiz. **38**, 316 (1988) [Sov. J. Nucl. Phys. **38**, 188 (1983)].
[27] P.F. Bortignon and R.A. Broglia, Nucl. Phys. **A371**, 405 (1981).
[28] M. Baranger, Nucl. Phys. **A149**, 225 (1970).
[29] D. Bes, G. Dussel, R. Broglia, R. Liotta, and B. Mottelson, Phys. Lett. **52B**, 253 (1974); D. Bes, G. Dussel, R. Broglia, R. Liotta, R. Perazzo, and H. Sofia, Nucl. Phys. **A260**, 1 (1976); **A260**, 27 (1976); **A260**, 77 (1976).
[30] P. Bortignon, R. Broglia, and D. Bes, Phys. Lett. **76B**, 153 (1978).
[31] G. Dussel, R. Perazzo, S. Reich, and H. Sofia, Nucl. Phys. **A401**, 1 (1983).
[32] G. Dussel, R. Perazzo, and H. Sofia, Phys. Rev. C **43**, 1211 (1991).
[33] P.F. Bortignon, R.A. Broglia, G.F. Bertsch, and J. Pacheco, Nucl. Phys. **A460**, 149 (1986).